# CHAPTER 3 TEST DESIGN

## 3.1 Facility and coordinate systems

### 3.1.1 Towing Tank

Tests are conducted at the IIHR towing tank shown in Fig. 3-1. The tank is 100 m long, 3.048 m wide and 3.048 m deep, and equipped with a drive carriage, PMM carriage, Krypton camera module, automated wave dampener system, and wave-dampening beach. The drive carriage is instrumented with several data-acquisition computers, speed circuit, and signal conditioning for analog voltage measurements of such as forces and moments, ship motions, and carriage speed. The drive carriage pulls the PMM carriage that is used as a point of attachment for model 5512. The Krypton camera module, an infrared-camera-based motion tracking system, tracks the dynamic motions of the model. Wave dampeners and the wave-dampening beach enable twelve-minute intervals between carriage runs that is determined sufficient based on visual inspection of the free surface.

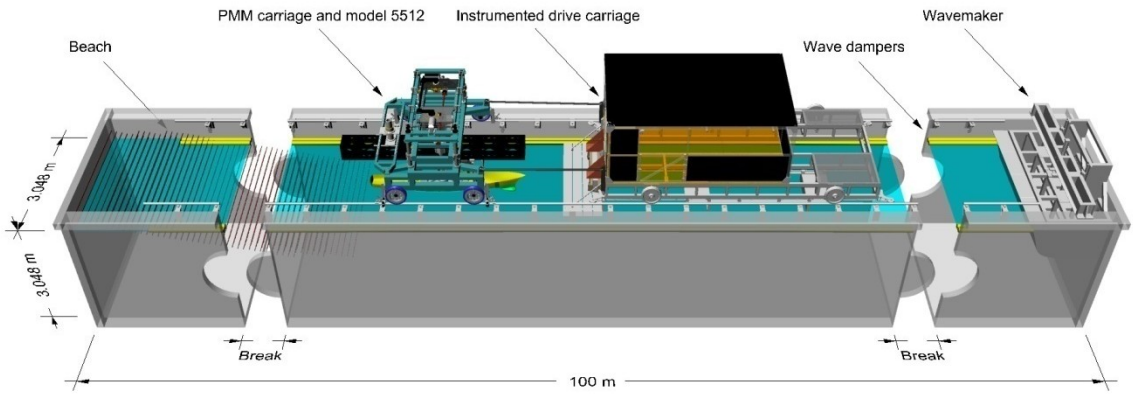


Figure 3-1 IIHR towing tank facility and maneuvering experimental setup.

### 3.1.2 PMM

Design and construction of the PMM is a collaborative effort by Sanshin Seisaku-sho Ltd. and Mori Engineering Ltd. for the mechanical and electrical systems, respectively. A four-wheel carriage supports the main PMM mechanical system that is towed behind the IIHR drive carriage. The mechanical system is a scotch-yoke type which converts rotational motion of an 11 kW AC servo motor to linear sway motion of a sway box and angular yaw motion of a yaw platter beneath the sway box (Fig. 3-2). The scotch yoke is driven through a control rack, PC, and software up to 0.25 Hz with maximum sway and yaw amplitudes of ±500 mm and ±30°, respectively. Two types of strongback, long (4 m) and short (1.5 m), are attached to the yaw platter for fixed- and free-mount conditions (See Section 3.2), respectively. Each strongback is pre-settable at drift angle $\beta$ between ±30°. Factory calibrated linear and rotational potentiometers are installed on the PMM carriage to monitor and report the sway and yaw positions of the sway box and yaw platter, respectively. Static calibrations of the linear potentiometers are conducted periodically to check their output.

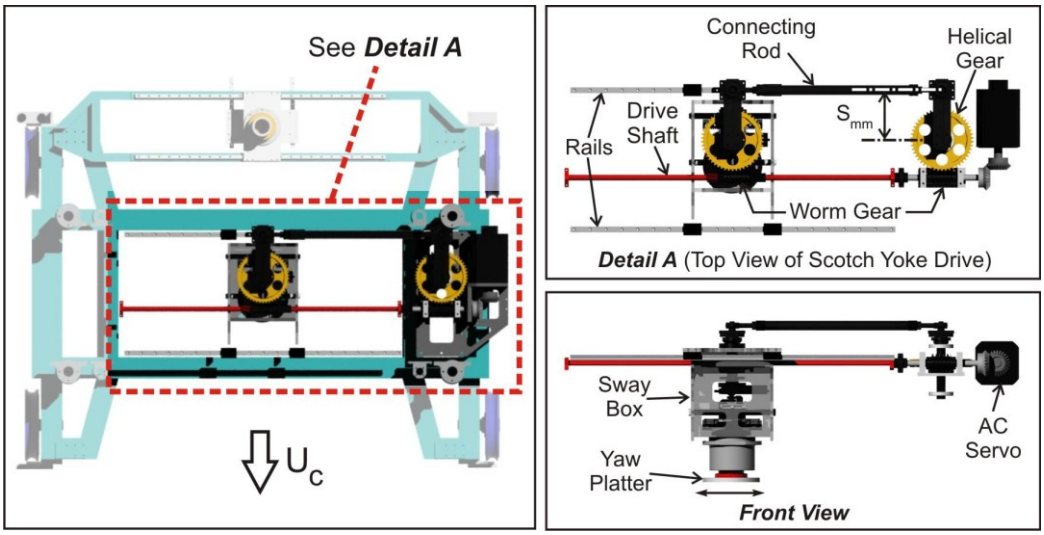


Figure 3-2 Top view of PMM carriage (top left), close up of the scotch yoke drive (top right), and towing tank PMM test coordinate systems (bottom).

### 3.1.3 Coordinate systems

The Earth-fixed (or the Towing-tank-fixed) $x_E$-$y_E$ coordinate system (See Fig. 3-3) can be fixed at any arbitrary position in the towing tank, with its longitudinal axis $x_E$ aligned with the towing tank centerline and pointed to the towing direction.

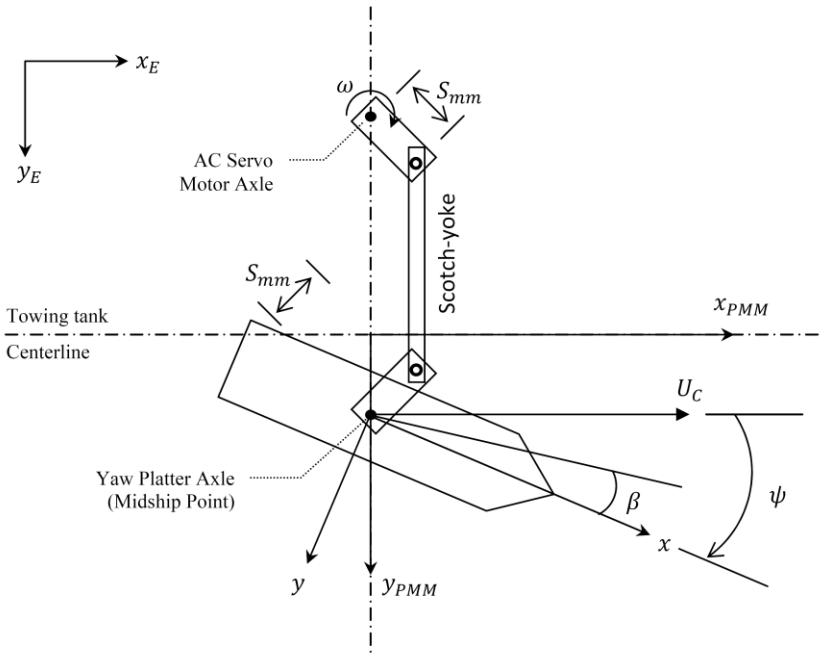


Figure 3-3 Coordinate systems for PMM test (Not scaled).

PMM-fixed $x_{PMM}$-$y_{PMM}$ coordinate system (See Fig. 3-3) is fixed at the PMM carriage, traveling at a constant speed $U_C$, with its lateral axis $y_{PMM}$ placed normal to the towing tank centerline. PMM motions for the Sanshin PMM carriage basically can be described in the PMM-fixed coordinate system by five quantities. These include 1) the carriage speed $U_C$, 2) sway crank amplitude $S_{mm}$, 3) yaw motion amplitude $\psi_{\max}$, 4) drift angle $\beta$, and 5) the number of PMM rotations per minute N. The following relations are used to setup static and dynamic tests according to the test conditions:

$$y_{PMM} = -2S_{mm} \sin \omega t \tag{3.1a}$$

$$v_{PMM} = -2S_{mm}\, \omega \cos \omega t \tag{3.1b}$$

$$\dot{v}_{PMM} = 2S_{mm}\, \omega^2 \sin \omega t \tag{3.1c}$$

$$\psi = -\psi_{max} \cos \omega t + \beta \tag{3.1d}$$

$$r_{PMM} = \psi_{max}\, \omega \sin \omega t \tag{3.1e}$$

$$\dot{r}_{PMM} = \psi_{max}\, \omega^2 \cos \omega t \tag{3.1f}$$

where, $\omega = 2\pi \mathrm{N}/60$.

Ship-fixed $x$-$y$ coordinate system is fixed at the midship point of the model with its *x* and *y* coordinates aligned with the model longitudinal and lateral directions, respectively, and pointing to upstream and to the starboard side, respectively (See Fig. 3-3). The ship motion parameters such as model velocities and accelerations (at the midship point) in the ship-fixed coordinate system can be written using (2.7) as following:

$$u = U_C \cos \psi + v_{PMM} \sin \psi \tag{3.2a}$$

$$\dot{u} = \dot{v}_{PMM} \sin \psi + r(v_{PMM} \cos \psi - U_C \sin \psi) \tag{3.2b}$$

$$v = v_{PMM} \cos \psi - U_C \sin \psi \tag{3.2c}$$

$$\dot{v} = \dot{v}_{PMM} \cos \psi - r(U_C \cos \psi + v_{PMM} \sin \psi) \tag{3.2d}$$

$$r = r_{PMM} \tag{3.2e}$$

$$\dot{r} = \dot{r}_{PMM} \tag{3.2f}$$

Note that the carriage acceleration is assumed to be zero, i.e. $\dot{U}_C = \dot{u}_E = 0$. The motion parameters in (3.2) are shown as dimensional while those can be non-dimensionalized using the *Prime-System* shown in (2.26) when necessary.

For the PIV applications of the PMM, the PMM-fixed $x_{PMM}$-$y_{PMM}$ coordinate system that is advancing forward with $U_C$ is considered as stationary, instead an incoming

free stream velocity $U_C$ is assumed, as depicted in Fig. 3-4. In the figure, the PMM-fixed $x_{PMM}$ and $y_{PMM}$ coordinates are re-designated as $X$ and $Y$, respectively, and the direction of $X$ coordinate is reverted from Fig. 3-3, pointing to downstream . Then, the PMM motion equations (3.1a) and (3.1d) are re-described as

$$Y = -Y_0 \sin \omega t \tag{3.3a}$$

$$\psi = -\psi_0 \cos \omega t \tag{3.3b}$$

respectively, where $Y_0$ and $\psi_0$ are renamed from $2S_{mm}$ and $\psi_{max}$ in (3.1a) and (3.1d), respectively, and for (3.3b) the drift angle $\beta$ in (3.1d) is set to zero. Accordingly, the sway velocity and the yaw rate, with designated as $V_P$ and $r$, respectively, are written as

$$V_P = -Y_0 \omega \cos \omega t \tag{3.4a}$$

$$r = \psi_0 \omega \sin \omega t \tag{3.4b}$$

by re-describing the equations (3.1b) and (3.1e), respectively.

In Fig. 3-4, the ship-fixed $x$-$y$ coordinate system is fixed at the forward perpendicular (FP) position and the direction of the $x$ coordinate is reverted from that in Fig. 2-3, pointing to the stern side of the model. Then, as the model is undergoing a reciprocal lateral sway motion $Y$ and an angular yaw motion $\psi$ with pivoted at the midship point ($x_0$,$y_0$), as per the equations (3.3a) and (3.3b), respectively, the free stream velocity $U_C$ can be described in the ship-fixed coordinate system. For a field point $P$($x$,$y$) shown in Fig. 8, the free stream velocity components in $x$ and $y$ directions of the ship-fixed coordinate system, with designated as $u_P$ and $v_P$, respectively, are written as

$$u_P = U_C \cos \psi + V_P \sin \psi - r \cdot dy \tag{3.5a}$$

$$v_P = -U_C \sin \psi + V_P \cos \psi + r \cdot dx \tag{3.5b}$$

where

$$dx = x - x_0 \tag{3.6a}$$

$$dy = y - y_0 \tag{3.6b}$$

and $(x_0, y_0) = (0.5L, 0)$ , where $L$ is the model length, is the mid-ship location or the yaw motion pivot point in the ship-fixed coordinate system.

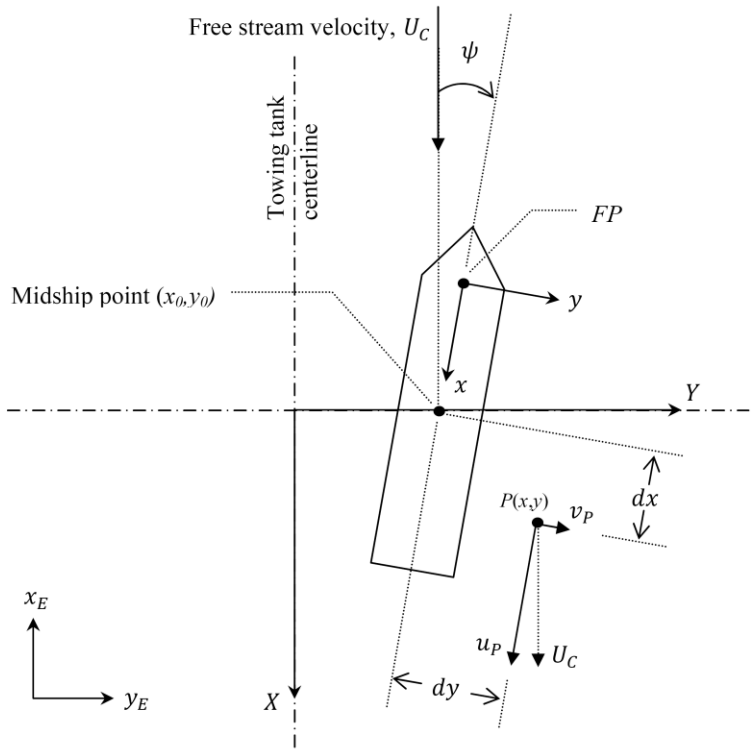


Figure 3-4 Coordinate systems for PIV test (Not scaled).

## 3.2 Model

The model geometry is DTMB model 5512 (Fig. 3-5), a 1:46.6 scale, $L_{PP}$ = 3.048 m, fiber-reinforced Plexiglas hull with block coefficient, $C_B$ = 0.506. DTMB model 5512 is a geosim of DTMB model 5415, which is a 1:24.8 scale, $L_{PP}$ = 5.72 m model of the U.S. Navy's pre-contract design for a surface combatant (DDG-51) ca. 1980 with a sonar dome bow and transom stern. The model was manufactured at the Naval Surface Warfare Center (NSWC) of USA Navy. The model is un-appended except for port and starboard bilge keels, i.e., not equipped with shafts, struts, propulsors, or rudders. To initiate transition to turbulent flow, a row of cylindrical studs of 1.6 mm height and 3.2 mm diameter are fixed with 9.5 mm spacing at $x$ = 0.45 ($x$ = 0 at the mid-ship, forward positive). The stud dimensions and placement on the model are in accordance with the recommendations by the 23rd ITTC (ITTC, 2002).


Figure 3-5 Photographs of DTMB model 5512. The top view highlights the bilge keels.

Table 3-1 Full- and model-scale particulars.

| | | Ship | IIHR | | FORCE | INSEAN |
|---|---|---|---|---|---|---|
| | | | Fix mount | Free mount | | |
| Scale | - | 1 : 1 | 1 : 46.588 | | 1:35.48 | 1:24.83 |
| $L$ ($L_{PP}$) | m | 142.00 | 3.048 | | 4.0023 | 5.7200 |
| $L_{WL}$ | m | 142.18 | 3.052 | | 4.0083 | 5.7273 |
| $B_{WL}$ | m | 19.10 | 0.410 | | 0.5382 | 0.7690 |
| $T$ ($T_m$) | m | 6.16 | 0.136 | | 0.1736 | 0.2480 |
| $\nabla$ | $m^3$ | 8472 | 0.086 | | 0.1897 | 0.5540 |
| $\Delta$ | Ton | 8684 | 0.086 | | 0.1897 | 0.5540 |
| $C_b$ | - | 0.506 | 0.506 | | 0.506 | 0.506 |
| $m$ | Kg | | 83.35 | 82.55 | 235.9 | N/A |
| $x_G$ | m | | -0.0157 | | | N/A |
| $y_G$ | m | | 0.0000 | | | N/A |
| $z_G$ | m | | N/A | 0.084 | N/A | N/A |
| $I_x$ | $Kg{\cdot}m^2$ | | N/A | 1.98 | N/A | N/A |
| $I_y$ | $Kg{\cdot}m^2$ | | N/A | 53.88 | 225.3 | 1151.4 |
| $I_z$ | $Kg{\cdot}m^2$ | | 44.35 | 49.99 | 235.9 | N/A |

Model- and full-scale geometric parameters for 5512 are summarized in Table 3-1. The length between perpendiculars $L_{PP}$, length at the design waterline $L_{WL}$, beam at the design waterline $B_{WL}$, mean draft $T_m$, volume $\nabla$, displacement $\Delta$, block coefficient $C_B$, and the longitudinal and transverse center of gravity (COG) $x_G$ and $y_G$ are provided by NSWC. Total mass $m$ of the model is a sum of element mass parts including the bare model (shell), several ballast weights, and several fixing parts for model mounting. The vertical COG $z_G$ is determined using the added ballast method as per M. Irvine et al. (2008). The moments of inertia in roll and pitch $I_x$ and $I_y$ are determined using the pendulum method as well per M. Irvine et al. (2008) by measuring the roll and pitch gyradius, respectively. The yaw moment of inertia $I_z$ is determined by using a forced-yaw method[6]. Lastly, the FORCE and INSEAN model scale particulars are as well included in Table 3-1.

[6] Model is placed in air and forced to oscillate sinusoidally in yaw with known amplitude $\psi$ and frequency $\omega$ to measure the yaw moment $M_z$. Then, the yaw moment of inertia $I_z$ can be determined from the relation $M_z = I_z \cdot \dot{r}$, where $\dot{r} = \psi\omega^2$ and $I_z$, for a set of combinations of $\psi$ and $\omega$ using such as a least-square-error method.

### 3.3 Mount and Mount Conditions

Model is installed to PMM using two types of mount, fix- or free-mount shown in Fig. 3-6 (a) and (b), respectively. The fix-mount constrains the model in all motions, whereas the free-mount allows the model to move freely in selective motions such as heave, pitch, and roll. The free-mount consists of the short strongback and a combination of three balances, the fore, midship, and aft balances that are identical in shape. Each balance is a crank-assembly with counter weights (colored in yellow in the figure) for a neutral angular moment of each crank part. The balances allow the model to move freely in heave and pitch while the mid balance (placed in normal direction with respect to the other balances) prevents the relative surge motion of the model while towed. At the end of each balance, two types of joints using roller or spherical bearings are used for model connection; the former prevents and the latter allows the roll motion, respectively, while transmitting the heave and pitch motions of the model.

Tests are carried out four mount conditions: 1) fixed at evenkeel ($FX_0$); 2) fixed sunk and trim ($FX_{\sigma\tau}$); 3) free to heave and pitch ($FR_{z\theta}$); and 4) free to heave, pitch and roll ($FR_{z\theta\phi}$). The $FX_0$ and $FX_{\sigma\tau}$ mount conditions are the model installations using the fix-mount (fixed-model setup, Fig. 3-6c). For the installations, the model is first assembled rigidly with the fix-mount and then ballasted to the static waterline position for the $FX_0$ condition and to the dynamic sinkage ($\sigma = 0.192 \times 10^{-2}\, L$) and trim ($\tau = -0.136°$, bow down) corresponding to $Fr = 0.280$ for the $FX_{\sigma\tau}$ condition, respectively. The $FR_{z\theta}$ and $FR_{z\theta\phi}$ mount conditions are using the free-mount (free-model setup, Fig. 3-6d). Model is first ballasted to the static waterline and then connected to the free-mount using the roller joint for the $FR_{z\theta}$ condition and using the spherical joint for the $FR_{z\theta\phi}$ condition, respectively. A summary of the mount conditions are presented in Table 3-2.

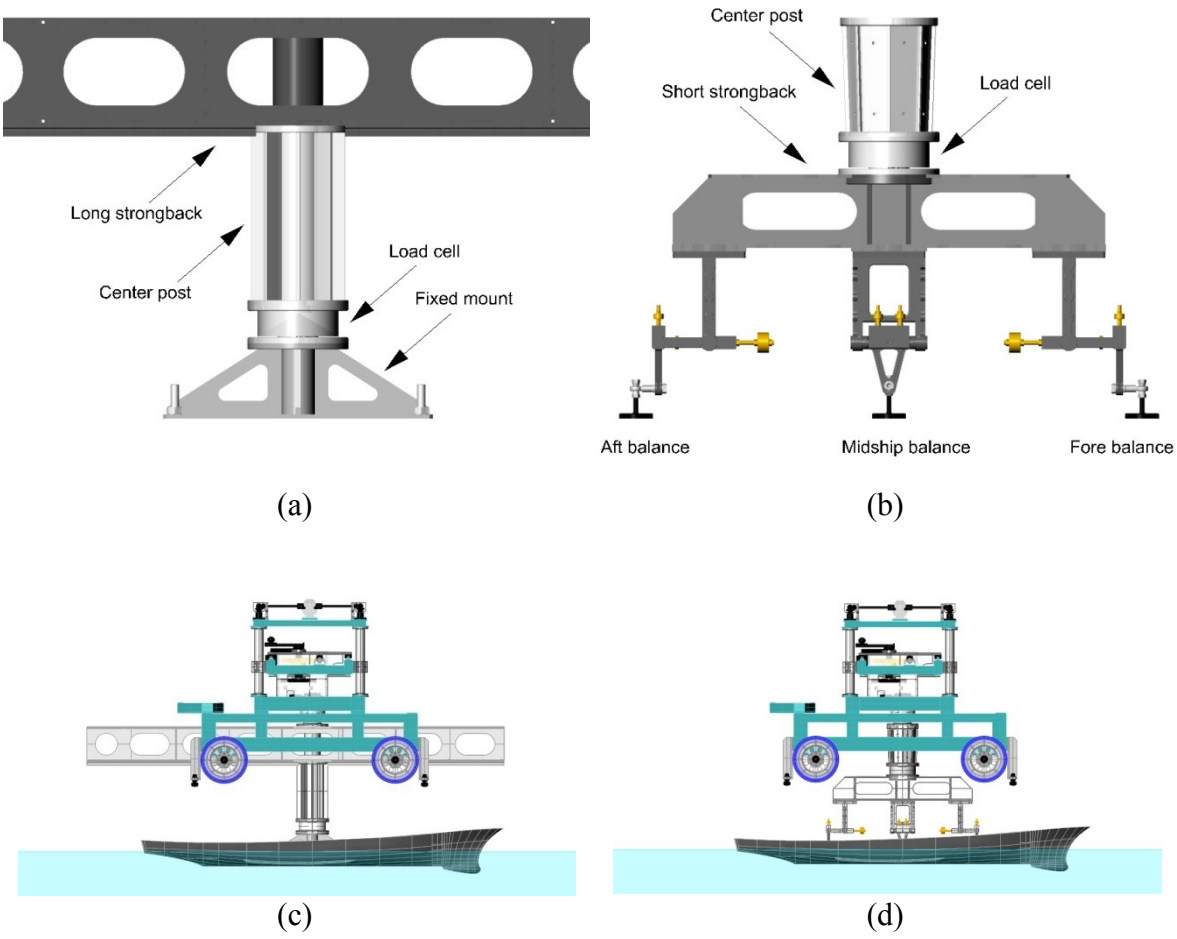


Figure 3-6 Sideviews show: (a) fixed- and (b) free-mounts, and (c) fixed- and (d) free-model setups.

Table 3-2 Mount Conditions.

| Motion | Mount conditions | | | |
|---|---|---|---|---|
| | $FX_0$ | $FX_{\sigma\tau}$ | $FR_{z\theta}$ | $FR_{z\theta\phi}$ |
| Surge ($x$) | Forced | Forced | Forced | Forced |
| Sway ($y$) | Forced | Forced | Forced | Forced |
| Yaw ($\psi$) | Forced | Forced | Forced | Forced |
| Heave ($z$) | Fixed at 0.0 | Fixed at $1.9209\times10^{-3}L$ | Free | Free |
| Pitch ($\theta$) | Fixed at 0.0 | Fixed at -0.136° | Free | Free |
| Roll ($\phi$) | Fixed at 0.0 | Fixed at 0.0 | Fixed at 0.0 | Free |

## 3.4 Test Conditions

Test conditions are summarized in Table 3-3. Static drift tests are conducted at three towing speeds corresponding to $Fr$ = 0.138, 0.280, and 0.410, which are the low, medium, and high $Fr$ condition, respectively. For low and medium $Fr$ conditions, drift angle $\beta$ values are varied between ±20°, whereas between ±12° for the high $Fr$ condition limited by the capacity of load-cell. The largest drift angle values correspond to sway velocities $v$ = 0.342 and 0.208, respectively. The angles are distributed symmetrically with respect to the $\beta = 0°$ line, i.e. the model towing direction, but distributed unevenly with clustered around $\beta$ = ±10°. Pure sway tests are carried out at medium $Fr$ only and at three maximum drift angles $\beta_{max}$ = 2°, 4°, 10° which correspond to the maximum sway velocity values $v_{max}$ = 0.035, 0.070, 0.174, respectively. Pure yaw tests are carried out for all three $Fr$ cases, at six maximum yaw rates $r_{\max}$ = 0.05, 0.15, 0.30, 0.45, 0.60, and 0.75 for low and medium $Fr$ cases and at first four maximum yaw rates for high $Fr$ case, respectively, again limited by load-cell capacity. Yaw and drift tests are carried out for medium $Fr$ case only and at three drift angles $\beta$ = 9°, 10°, and 11° with the maximum yaw rate fixed at $r_{\max}$ = 0.3.

Sway motion amplitude $2S_{mm}$, yaw motion amplitude $\psi_{\max}$, and drift angle $\beta$ used in (3.1) are determined to yield the motion parameters such as sway $v_{\max}$, $\dot{v}_{\max}$ and $r_{\max}$, $\dot{r}_{\max}$ with considerations of minimizing interferences between the PMM motions and the tank walls. PMM motion frequency N values are determined to avoid possible hydrodynamic effects such as tank resonance and memory effects associated with the dynamic tests. Typically, PMM motion frequencies are restricted in terms of three non-dimensional frequencies: $\omega_1 = \omega L/U_C$, $\omega_2 = \omega\sqrt{L/g}$, and $\omega_3 = \omega U_C/g$, where $\omega$ is the PMM motion frequency and $g$ is the local value of gravity. $\omega_1$ is related to non-stationary lift and memory effects (Nomoto 1975, Wagner Smitt & Chislett 1974, Milanov 1984, van Leeuwen 1969), $\omega_2$ is related to tank resonance, and $\omega_3$ is related to un-

realistic combinations of pulsation and translation (Brard 1948, Wehausen & Laitone 1960, van Leeuwen 1964). The ITTC Recommended Procedures and Guidelines 7.5-02-06-02.2 'Captive Model Test Procedures' recommends $\omega_1 = 1 \sim 4$, $\omega_2 = 0.15 \sim 0.2$, and $\omega_3 \ll 0.25$, however, the PMM motion frequencies in the present tests are $\omega_1 = 1.14 \sim 3.13$, $\omega_2 = 0.27 \sim 0.88$, and $\omega_3 = 0.04 \sim 0.34$ due to the facility limitations regarding dimensions and capabilities.

Tests are repeated 12 times at selected conditions (marked as bold characters) for the purpose of uncertainty analysis (UA) presented in Chapter 5. UA cases include $\beta$ = ±10° for static drift test, $\beta_{max}$ = 10° for pure sway test, $r_{max}$ = 0.3 for pure yaw test, and $\beta$ = 10° for yaw and drift test. For $FX_0$ and $FR_{z\theta}$ conditions, all the test cases listed in Table 3-3 are carried out. For $FX_{\sigma\tau}$ condition, test cases include static drift test at all *Fr* conditions and pure sway and pure yaw tests at the medium *Fr* conditions. For $FR_{z\theta\phi}$ condition, static drift test at all *Fr* and dynamic tests only at the UA cases.

PIV measurements are for pure sway and pure yaw tests. Both of the pure sway and pure yaw tests are carried out at the $FR_{\sigma\tau}$ mount condition and at Fr = 0.280. Test cases are highlighted in Table 3-3.

Table 3-3 PMM Test conditions.

| Test | $Fr$ | $U_C$ | $\beta$ | $\frac{y_{max}}{L}$ | $\frac{v_{\max}}{U_C}$ | $\frac{\dot{v}_{\max} L}{U_C^2}$ | $\beta_{\max}$ | $\psi_{\max}$ | $\frac{r_{\max} L}{U_C}$ | $\frac{\dot{r}_{\max} L}{U_C^2}$ | $\frac{\omega L}{U_C}$ | Mount condition |
|---|---|---|---|---|---|---|---|---|---|---|---|---|
| | | (m/s) | (°) | (-) | (-) | (-) | (°) | (°) | (-) | (-) | (-) | |
| Static drift | 0.138 | 0.754 | -20, -16, -12, -11, **-10**‡, -9, -6, -2, 0, 2, 6, 9, **10**†, 11, 12, 16, 20 | 0 | 0 | 0 | - | 0 | 0 | 0 | 0 | **$FX_0$, $FR_{z\theta}$, $FR_{z\theta\phi}$** |
| | 0.280 | 1.531 | -20, -16, -12, -11, **-10**‡, -9, -6, -2, 0, 2, 6, 9, **10**†, 11, 12, 16, 20 | 0 | 0 | 0 | - | 0 | 0 | 0 | 0 | **$FX_0$, $FX_{\sigma\tau}$, $FR_{z\theta}$, $FR_{z\theta\phi}$** |
| | 0.410 | 2.241 | -12, -11, **-10**‡, -9, -6, -2, 0, 2, 6, 9, **10**†, 11, 12 | 0 | 0 | 0 | - | 0 | 0 | 0 | 0 | **$FX_0$, $FR_{z\theta}$, $FR_{z\theta\phi}$** |
| Pure sway | 0.280 | 1.531 | 0 | 0.021 | 0.035 | 0.058 | 2 | 0 | 0 | 0 | 1.672 | $FX_0$, $FX_{\sigma\tau}$, $FR_{z\theta}$ |
| | | | 0 | 0.042 | 0.070 | 0.117 | 4 | 0 | 0 | 0 | 1.672 | $FX_0$, $FX_{\sigma\tau}$, $FR_{z\theta}$ |
| | | | **0** | **0.104** | **0.174** | **0.291** | **10** | **0** | **0** | **0** | **1.672** | **$FX_0$, $FX_{\sigma\tau}$, $FR_{z\theta}$, $FR_{z\theta\phi}$** |
| Pure yaw | 0.138 | 0.754 | 0 | 0.013 | 0 | 0 | - | 1.5 | 0.05 | 0.10 | 0.956 | $FX_0$, $FR_{z\theta}$ |
| | | | 0 | 0.040 | 0 | 0 | - | 4.4 | 0.15 | 0.29 | 0.956 | $FX_0$, $FR_{z\theta}$ |
| | | | **0** | **0.080** | **0** | **0** | **-** | **8.8** | **0.30** | **0.58** | **0.956** | **$FX_0$, $FR_{z\theta}$, $FR_{z\theta\phi}$** |
| | | | 0 | 0.120 | 0 | 0 | - | 13.1 | 0.45 | 0.87 | 0.956 | $FX_0$, $FR_{z\theta}$ |
| | | | 0 | 0.104 | 0 | 0 | - | 14.2 | 0.60 | 1.49 | 1.194 | $FX_0$, $FR_{z\theta}$ |
| | | | 0 | 0.128 | 0 | 0 | - | 17.2 | 0.75 | 1.82 | 1.194 | $FX_0$, $FR_{z\theta}$ |
| | 0.280 | 1.531 | 0 | 0.018 | 0 | 0 | - | 1.7 | 0.05 | 0.08 | 1.672 | $FX_0$, $FX_{\sigma\tau}$, $FR_{z\theta}$ |
| | | | 0 | 0.054 | 0 | 0 | - | 5.1 | 0.15 | 0.25 | 1.672 | $FX_0$, $FX_{\sigma\tau}$, $FR_{z\theta}$ |
| | | | **0** | **0.107** | **0** | **0** | **-** | **10.2** | **0.30** | **0.50** | **1.672** | **$FX_0$, $FX_{\sigma\tau}$, $FR_{z\theta}$, $FR_{z\theta\phi}$** |
| | | | 0 | 0.099 | 0 | 0 | - | 12.0 | 0.45 | 0.98 | 2.150 | $FX_{\sigma\tau}$, $FR_{z\theta}$ |
| | | | 0 | 0.046 | 0 | 0 | - | 8.2 | 0.45 | 1.41 | 3.127 | $FX_0$ |
| | | | 0 | 0.130 | 0 | 0 | - | 15.6 | 0.60 | 1.29 | 2.150 | $FX_{\sigma\tau}$, $FR_{z\theta}$ |
| | | | 0 | 0.061 | 0 | 0 | - | 10.9 | 0.60 | 1.88 | 3.127 | $FX_0$ |
| | | | 0 | 0.124 | 0 | 0 | - | 17.2 | 0.75 | 1.93 | 2.502 | $FX_{\sigma\tau}$, $FR_{z\theta}$ |
| | | | 0 | 0.077 | 0 | 0 | - | 13.5 | 0.75 | 2.35 | 3.127 | $FX_0$ |
| | 0.410 | 2.241 | 0 | 0.038 | 0 | 0 | - | 2.5 | 0.05 | 0.06 | 1.672 | $FX_0$, $FR_{z\theta}$ |
| | | | 0 | 0.115 | 0 | 0 | - | 7.5 | 0.15 | 0.17 | 1.672 | $FX_0$, $FR_{z\theta}$ |
| | | | **0** | **0.072** | **0** | **0** | **-** | **8.4** | **0.30** | **0.61** | **2.986** | **$FX_0$, $FR_{z\theta}$, $FR_{z\theta\phi}$** |
| | | | 0 | 0.108 | 0 | 0 | - | 12.5 | 0.45 | 0.92 | 2.986 | $FX_0$, $FR_{z\theta}$ |
| Yaw and drift | 0.280 | 1.531 | 9 | 0.107 | 0 | 0 | - | 10.2 | 0.30 | 0.50 | 1.672 | $FX_0$, $FR_{z\theta}$ |
| | | | **10** | **0.107** | **0** | **0** | **-** | **10.2** | **0.30** | **0.50** | **1.672** | **$FX_0$, $FR_{z\theta}$, $FR_{z\theta\phi}$** |
| | | | 11 | 0.107 | 0 | 0 | - | 10.2 | 0.30 | 0.50 | 1.672 | $FX_0$, $FR_{z\theta}$ |

**Bold**: UA cases with 12 repeat tests; † UA cases for $FX_0$ and $FX_{\sigma\tau}$ conditions; ‡ UA cases for $FR_{z\theta}$ and $FR_{z\theta\phi}$ conditions.
Highlighted: PIV conditions.

## 3.5 Data Acquisition and Reduction Methodology

### 3.5.1 Forces and Moment and Motions

The present interest is in data acquisition of carriage speed $U_C$, forces and moments ($F_x$, $F_y$, $F_z$, $M_x$, $M_y$, $M_z$), and ship model motions ($x_{PMM}$, $y_{PMM}$, $z_{mm}$, $\phi$, $\theta$, $\psi$) for static and dynamic PMM tests. All variables are acquired as time histories through each carriage run. Static test variables ($F_x$, $F_y$, $M_z$, $z_{mm}$, $\theta$, $\phi$) are time-averaged whereas dynamic test variables ($F_x$, $F_y$, $M_z$, $y_{PMM}$, $z_{mm}$, $\phi$, $\theta$, $\psi$) are treated with harmonic analysis in the data reduction phases of the study which is explained in further detail below. $y_{PMM}$, $z_{mm}$, $\phi$, $\theta$, and $\psi$ are measured only for free-model condition tests. Although not used in the data-reduction equations, $x_{PMM}$, $F_z$, $M_x$, $M_y$ are also measured to monitor operation of the mount and loadcell. The measurement details for $U_C$ are presented in Longo and Stern, (2005). First, the data reduction equations for static and dynamic PMM tests are presented followed by the data-reduction methodology.

The data reduction equations (DRE's) for hydrodynamic forces and moment are:

$$X = \frac{F_x + m\left(\dot{u} - vr - x_G r^2 - y_G \dot{r}\right)}{\frac{1}{2}\rho (u^2+v^2) LT} \tag{3.7a}$$

$$Y = \frac{F_y + m\left(\dot{v} + ur - y_G r^2 + x_G \dot{r}\right)}{\frac{1}{2}\rho (u^2+v^2) LT} \tag{3.7b}$$

$$N = \frac{M_z + I_z \dot{r} + m\left(x_G(\dot{v}+ur) - y_G(\dot{u}-vr)\right)}{\frac{1}{2}\rho (u^2+v^2) L^2 T} \tag{3.7c}$$

where $y_G$ is assumed as non-zero from equations (2.1) for the purpose of uncertainty analysis in Section 5.1. Although the equations (3.7) are technically applicable DRE's for all tests herein, they can be simplified considerably by dropping the inertia terms for the case of static drift tests, which is done below in equations (3.8).

$$X = \frac{F_x}{\frac{1}{2}\rho U_C^2 LT} \tag{3.8a}$$

$$Y = \frac{F_y}{\frac{1}{2}\rho U_C^2 LT} \tag{3.8b}$$

$$N = \frac{M_z}{\frac{1}{2}\rho U_C^2 L^2 T} \tag{3.8c}$$

The PMM motion parameters $u$, $v$, $r$, $\dot{u}$, $\dot{v}$, and $\dot{r}$ in (3.7) are derived from the measured sway displacement $y_{PMM}$ and yaw angle $\psi$ data by using the coordinate transformations between the ship-fixed and PMM-fixed reference frames shown in (3.2). For this, first, time histories of the $y_{PMM}$ and $\psi$ data are FS reconstructed by using (3.11) for $\chi = y_{PMM}$ and $\psi$, respectively, and then $v_{PMM}$, $\dot{v}_{PMM}$ and $r_{PMM}$, $\dot{r}_{PMM}$ are obtained through successive differentiations of the $\chi$'s with respect to time $t$, respectively. The motions data, heave $z$, pitch $\theta$, and roll $\phi$ are not reduced except for the nondimensionalization of $z$ with the ship length $L$,

$$z = \frac{z_{mm}}{L} \tag{3.9}$$

where the $z_{mm}$ is dimensional heave data as measured in mm unit.

For dynamic tests, time-histories of the data can be expressed in harmonic forms using a 6th-order Fourier-series (FS) equation as following:

$$\chi(t) = \chi_0 + \sum_{n=1}^{6}(\chi_{Sn} \sin n\omega t + \chi_{Cn} \cos n\omega t) \tag{3.10a}$$

where,

$$\chi_0 = \frac{1}{M}\sum_{i=1}^{M} \chi_i \tag{3.10b}$$

$$\chi_{Sn} = \frac{2}{M}\sum_{i=1}^{M} \chi_i \sin(n\omega t_i) \tag{3.10c}$$

$$\chi_{Cn} = \frac{2}{M}\sum_{i=1}^{M} \chi_i \cos(n\omega t_i) \tag{3.10d}$$

Here, $\chi$ is either $X$, $Y$, $N$, $z$, $\theta$, or $\phi$, subscript $n$ is the order of the FS, $M$ is the total number of data for FS, $\chi_i$ is the data sample at time $t_i$, $\omega$ is the PMM frequency, and $\chi_{Cn}$

and $\chi_{Sn}$ are the $n^{\text{th}}$-order cosine and sine harmonic amplitudes, respectively. Alternatively, (3.10) can also be expressed as

$$\chi(t) = \chi_0 + \sum_{n=1}^{6} \chi_n \cos\left(n\omega t + \varphi_{\chi n}\right) \tag{3.11a}$$

where

$$\chi_n = \sqrt{\chi_{Sn}^2 + \chi_{Cn}^2} \tag{3.11b}$$

$$\varphi_{\chi n} = -\arctan\left(\frac{\chi_{Sn}}{\chi_{Cn}}\right) \tag{3.11c}$$

where, $\chi_n$ and $\varphi_n$ are the $n^{\text{th}}$-order harmonic amplitude and phase, respectively, and $\chi_0$, $\chi_{Sn}$, and $\chi_{Cn}$ are as per (3.10).

### 3.5.2 Phase-Averaged Flow field

Data acquisition includes carriage speed $U_C$, PMM sway displacement $Y$ and yaw angle $\psi$, and the flow velocity components $U_i$ where $i$ = 1, 2, 3 for $U$, $V$, $W$, respectively. All variables are acquired at a number $N$ of phase $\gamma$ positions per each PMM cycle of frequency $f_{PMM}$, and a total number $L$ of data acquisitions during a carriage run where typically two and three quarters of PMM cycles are made. The nominal value of the phase position is given as $\gamma = (n-1)\cdot\Delta\gamma$ for $n$ = 1, …, $N$, where the phase interval $\Delta\gamma = 2\pi/N$. If $N$ = 32 phase positions per one PMM cycle, for example, a total $L$ = 88 data per one carriage run and a $\Delta\gamma$ = 11.25° of phase interval. The data acquisition procedure is repeated for a total number $K$ of carriage runs, accumulating data for the phase-averaging purpose.

The data acquisition time-point $t_{k,l}$ of the $l^{\text{th}}$ data from the $k^{\text{th}}$ carriage run is written as,

$$t_{k,l} = t_{0_k} + (l-1)\cdot\Delta t \tag{3.12}$$

for $k$ = 1, …, $K$ and $l$ = 1, …, $L$, where $t_{0_k}$ is the time when the first data sample of the $k^{\text{th}}$ carriage run is acquired and $\Delta t = (f_{PMM})^{-1}/N$ is the time interval between adjacent data samples. Subsequently, the $U_C$, $Y$, $\psi$, and $U_i$ data acquired at time $t_{k,l}$ are designated as $U_{C_{k,l}}$, $Y_{k,l}$, $\psi_{k,l}$, and $U_{i_{k,l}}$, respectively. The acquisition of $U_{C_{k,l}}$, $Y_{k,l}$, and $\psi_{k,l}$ data is the time-mean of twenty-five samplings of $U_C$, $Y$, and $\psi$ signal, respectively, for a short time period, a 100 μs, and the acquisition of $U_{i_{k,l}}$ is result from cross-correlation of the Stereo PIV image pairs take at time $t_{k,l}$.

The phase position $\gamma$ (not the nominal value but the actual value) at each data acquisition time $t_{k,l}$, designated as $\gamma_{k,l}$, may be found using the $Y_{k,l}$ and $\psi_{k,l}$ data from the equations (3a) and (3b) in Section 3.1.2, along with the relationship $\gamma = \omega t$, such that[7]

$$\gamma_{k,l} = \arctan\left(\frac{Y_{k,l}/Y_{0_k}}{\psi_{k,l}/\psi_{0_k}}\right) \tag{3.13}$$

where, $Y_{0_k}$ and $\psi_{0_k}$ are the sway and yaw motions amplitudes of the $k^{\text{th}}$ carriage run, respectively, evaluated using Fourier Series expressions of the $Y_{k,l}$ and $\psi_{k,l}$ data such that

$$Y_{0_k} = -\frac{2}{L_{FS}}\sum_{l=1}^{L_{FS}}\{Y_{k,l}\cdot\sin(\omega t_{k,l})\} \tag{3.14}$$

$$\psi_{0_k} = -\frac{2}{L_{FS}}\sum_{l=1}^{L_{FS}}\{\psi_{k,l}\cdot\cos(\omega t_{k,l})\} \tag{3.15}$$

where, $L_{FS} = n_{cycle}\cdot N$ and $n_{cycle}$ is the (integer) number of PMM cycles from the $k^{\text{th}}$ carriage run.

The PIV measured velocity data $U_{i_{k,l}}$ are normalized with the carriage speed $U_{C_{k,l}}$ measured at the same time instant, $t_{k,l}$, as

---

[7] For pure sway tests, where the yaw amplitude $\psi_0$ = 0 in equation (3.3b); the phase is $\gamma_{k,l} = \arcsin(-Y_{k,l}/Y_{0_k})$.

$$U_{i}^{*}{}_{k,l} = U_{i}{}_{k,l} / U_{C}{}_{k,l} \tag{3.16}$$

Note that, hereafter, the '*' symbol in (3.16) is omitted for simplicity as only the normalized velocity is of interest herein, otherwise mentioned. Then, the $U_{i}{}_{k,l}$ data are sorted into $N$ phase-groups by approximating the corresponding $\gamma_{k,l}$ value to the nearest nominal phase value, collecting a total number of $M$ data for each phase-group. Subsequently, the $U_{i}{}_{k,l}$ data are re-indexed as $U_{i}{}_{m,n}$ for $n = 1, \ldots, N$ and $m = 1, \ldots, M$, indicating the $m^{\text{th}}$ data of the $n^{\text{th}}$ phase-group.

For a given $n^{\text{th}}$ phase-group, the phase-averaged velocity component $\langle U_i \rangle$ can be computed from $U_{i}{}_{m,n}$ data such that

$$\langle U_i \rangle = \left( \sum_{m=1}^{M} U_{i}{}_{m,n} \right) / M \tag{3.17}$$

respectively for $i = 1, 2, 3$. Then, the turbulent velocity $u_i$ for $U_{i}{}_{n,m}$ data is defined as the deviation from the phase-averaged velocity $\langle U_i \rangle$ such as

$$u_{i}{}_{n,m} = U_{i}{}_{n,m} - \langle U_i \rangle \tag{3.18}$$

Next, the phase-averaged turbulent Reynolds stress at the $n^{\text{th}}$ phase is defined as the (co)variance between the turbulent velocity components and evaluated as

$$\langle u_i u_j \rangle = \left( \sum_{m=1}^{M} u_{i}{}_{n,m} \cdot u_{j}{}_{n,m} \right) / M \tag{3.19}$$

respectively for $i, j = 1, 2$, or 3. Note that, the '⟨ ⟩' symbol used for phase-averaged velocity $U_i$ in (3.17) and Reynolds stress $u_i u_j$ in (3.19) is omitted hereafter for simplicity.

Turbulent kinetic energy $k$ and axial vorticity $\omega_x$ are evaluated from the phase-averaged Reynolds stress $u_i u_j$ and velocity $U_i$ fields, respectively. The turbulent kinetic energy is defined as one half of the sum of the phase-averaged Reynolds stress components $u_i u_i$ such that

$$k = \frac{1}{2}(uu + vv + ww) \tag{3.20}$$

The axial vorticity is the spatial differentiations of the phase-averaged cross-plane velocity components such that

$$\omega_x = \frac{\partial W}{\partial y} - \frac{\partial V}{\partial z} \tag{3.21}$$

where $y$ and $z$ are both non-dimensional with the model length $L$. Note that the vorticity components in the transverse and vertical directions are not evaluated, as no longitudinal gradient information is available from the stereo PIV data.

On the other hand, the $U_C$, $Y$, and $\psi$ data are as well used to determine the free stream velocity components $u_P$ and $v_P$ (See Section 3.1.2) for the UA purposes in Section 5.2. For this, sway velocity $V_P$ and yaw rate $r$ are calculated from the $Y$ and $\psi$ data, respectively, from which $u_P$ and $v_P$ at a field point ($x$,$y$) are evaluated along with the $U_C$ and $\psi$ data as per the following equations

$$u_P = U_C \cos\psi + V_P \sin\psi - r \cdot dy \tag{3.5a}$$

$$v_P = -U_C \sin\psi + V_P \cos\psi + r \cdot dx \tag{3.5b}$$

respectively, derived in Section 3.1.2.

First, the mean carriage speed $U_C$ is calculated from the $U_{C\,k,l}$ data as

$$U_C = \left[\sum_{k=1}^{K}\left\{\left(\sum_{l=1}^{L} U_{C\,k,l}\right)/L\right\}\right]/K \tag{3.22}$$

where the inner averaging (for index $l$) corresponds to the mean carriage speed of each $k^{\text{th}}$ carriage run, and the outer averaging (for index $k$) corresponds to the mean of the all $K$ carriage runs.

Next, the $V_P$ and $r$ values at each PMM phase position $\gamma$ are evaluated as per the equations (3.3a) and (3.3b) in Section 3.1.2, respectively, and by using the relation $\gamma = \omega t$ as

$$V_P = -Y_0 \omega \cos\gamma \tag{3.23}$$

$$r = \psi_0 \omega \sin\gamma \tag{3.24}$$

where, $\omega = 2\pi f_{PMM}$ is the cyclic PMM frequency, and $Y_0$ and $\psi_0$ are the mean values of $Y_{0_k}$ in (3.14) and $\psi_{0_k}$ in (3.15), respectively, such that

$$Y_0 = \left(\sum_{k=1}^{K} Y_{0_k}\right)/K \tag{3.25}$$

$$\psi_0 = \left(\sum_{k=1}^{K} \psi_{0_k}\right)/K \tag{3.26}$$

The phase position $\gamma$ in (3.23) and (3.24) can be calculated similarly as (3.13) such that

$$\gamma = \arctan\left(\frac{Y/Y_0}{\psi/\psi_0}\right) \tag{3.27}$$

where $Y_0$ and $\psi_0$ are from (3.25) and (3.26), respectively. Lastly, the mean heading angle $\psi$ is as well by phase-sorting and re-indexing the $\psi_{k,l}$ data as $\psi_{m,n}$ and by averaging as

$$Y = \left(\sum_{m=1}^{M} Y_{m,n}\right)/M \tag{3.28}$$

$$\psi = \left(\sum_{m=1}^{M} \psi_{m,n}\right)/M \tag{3.29}$$

for each $n^{\text{th}}$ phase-group.

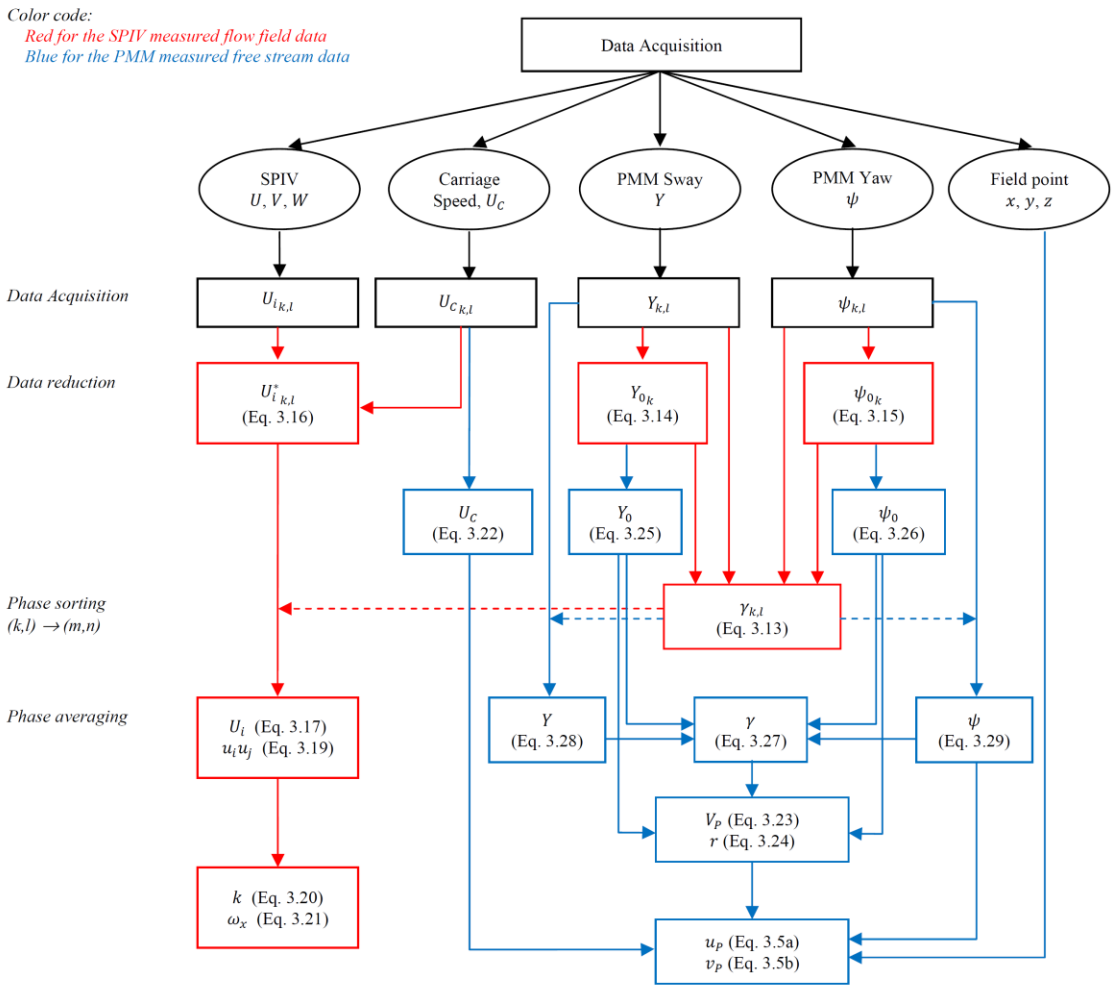


Figure 3-7 Data flow chart for data acquisition and reduction.

## 3.6 Measurement Systems and Calibration Procedures

### 3.6.1 Carriage Speed

Carriage speed is measured with an IIHR-designed and built speed circuit. The operating principle is integer pulse counting at a wheel-mounted encoder. The hardware consists of an 8000-count optical encoder, carriage wheel, sprocket pair and chain, analog-digital (AD) converter, and PC. Linear resolution of the encoder, sprocket pair and

chain, and wheel assembly is 0.15 mm/pulse. The speed circuit is periodically bench-calibrated to determine and adjust the frequency input/voltage output transfer function.

### 3.6.2 6-componet loadcell

Three forces and three moments are measured with an Izumi six-component strain-gage type loadcell, six Izumi amplifiers, 16-channel AD converter and PC. Maximum force and moment ranges are 500 N for $F_x$, $F_y$, $F_z$ and 50 N-m, 50 N-m, 200 N-m for $M_x$, $M_y$, $M_z$, respectively. During the tests, the loadcell is calibrated internally at the amplifiers periodically. After the tests, the loadcell is statically calibrated on a test stand using standard weights.

Figure 3-8 Izumi six-component load cell (left) and Izumi amplifiers (right).

### 3.6.3 Motion Tracker

Ship model motions are measured using a Krypton Electronic Engineering Rodym DMM motion tracker. The Rodym DMM is a camera-based measurement system that triangulates the position of a target in 3D space for contactless measurement and evaluation of 6DOF motions. The hardware consists of a camera module comprising three fixed CCD cameras, target with 1-256 light-emitting diodes (LED's), camera control unit,

hand-held probe with six LED's, and PC. Krypton software is used for system calibration, and data acquisition and reduction.

Figure 3-9 Krypton Electronic Engineering Rodym DMM motion tracker.

The camera module measurement volume is determined by the overlapping field of views of the three CCD cameras. The measurement volume is 17 $m^3$, pyramidal-shaped with a ±30° viewing angle, and divided into three accuracy zones: (1) 1.5-3.0 m distance from camera module, zone #1; (2) 3.0-5.0 m distance from camera module, zone #2; and (3) 5.0-6.0 m distance from camera module, zone #3. Performance assessment results for the Rodym DMM using standard coordinate metrology procedures (ISO 10360-II, VDI 2617) are published by Krypton in a camera verification report as ±0.1 mm, ±0.2 mm, ±0.3 mm in zones #1, #2, #3, respectively.

A target with one or more affixed LED's is calibrated with the camera module and hand-held probe. 6DOF ascii data is reported at various data rates (dependent on the number of target LED's) from the camera controller on six analog channels. A seventh analog channel is used to report visibility of the target during the tests to ensure an unobstructed view between the camera module and target as the ship model moves through its trajectory.

### 3.6.4 Stereo PIV

The stereo PIV is a LaVision Inc. custom-designed and built measurement system (Fig. 3-10). It consists of a 120 mJ Nd:Yag laser, submerged lightsheet generator, two 1600x1200 pixel cross-correlation cameras fitted with 50 mm f/1.8 lenses, and computer and software for data acquisition and reduction of PIV recordings. The lenses are equipped with motors for automatic remote focusing and aperture adjustments. The camera bodies are equipped with motors for automatic remote Scheimpflug angle adjustments.

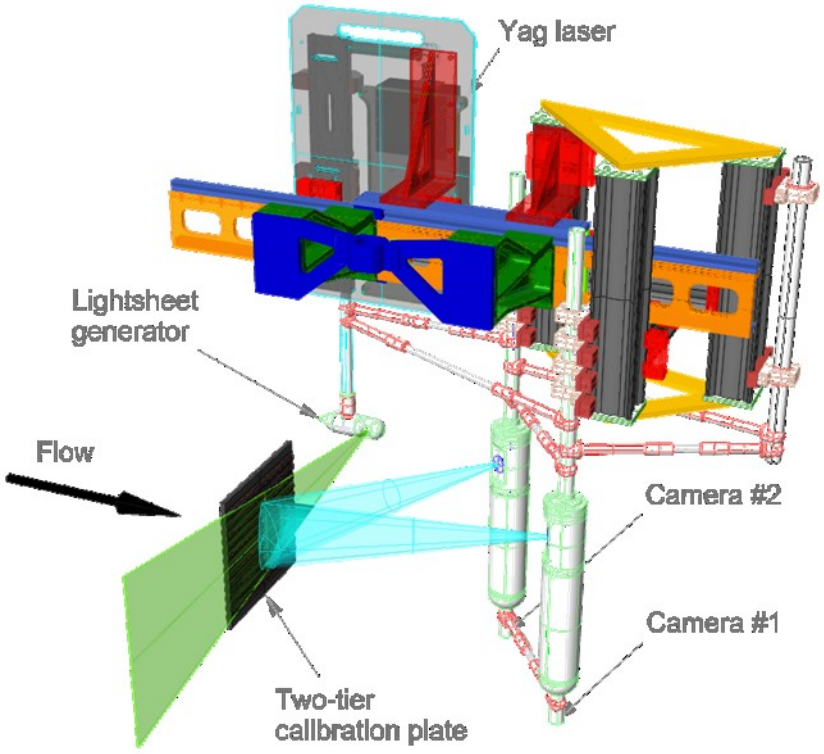


Figure 3-10 LaVision Stereo PIV System.

Both cameras are arranged asymmetrically in submerged enclosures downstream of the lightsheet to minimize wave and flowfield effects of the enclosures at the measurement area. The laser, lightsheet generator, and camera enclosures are assembled on a lightweight matrix of aluminum extrusions for adjustability and rigidity. The SPIV system is calibrated in situ by submerging and fixing a two-tier LaVision calibration plate in the plane of the lightsheet where both camera field of views overlap. Single images from each camera are used to create a mapping function of the plate markers which is used later to reconstruct 3D velocity vectors from particle image pairs. The original calibration is refined iteratively with a self-calibration procedure to account for translational or rotational misalignment of the calibration plate in the lightsheet plane.

## 3.7 Data Acquisition Procedures

### 3.7.1 Forces and Moments

#### 3.7.1.1 Data Acquisition Setup

The forces and moment experimental setup is as shown in Fig. 3-6 (c) and (d). For the fixed-model condition cases (Fig. 3-6c), the yaw platter supports a 4-m strongback, rigid post, load cell, fixed mount, and ship model and restrains all translations and rotations of the model. Sinkage and trim is set at the fixed mount for $FX_{\sigma\tau}$ condition cases at $Fr$ = 0.28. For the free-model condition cases (Fig. 3-6d), the yaw platter supports the loadcell, 1.5-m strongback, three balances that enable pitch, heave, and roll (fixed or free) motions and restrains surge, sway, yaw motions. Roll motion is enabled or disabled with spherical or one-degree-of-freedom connection bearings, respectively, at the fore and aft balances. In both fixed and free cases, model 5512 is mounted on the tank centerline at its design waterline (except for fixed tests with sinkage and trim) and either towed from $z$ = 0.01m (fixed) or $z$ = 0.0m (free). Force and moment data cables are run to six onboard amplifiers. For measuring sway position, a linear potentiometer is

fixed to the PMM carriage frame and linked to the sway box with wire loop, two pulley wheels, and bracket. For measuring yaw position, a rotational potentiometer is fixed inside the sway box and linked to the yaw platter with a wire loop. Data lines connect both potentiometers to amplifiers aboard the drive carriage.

The Krypton camera module is mounted backward-facing from the rear of the drive carriage for an unobstructed view of the LED target. The target is mounted near the bow and over the models centerline such that the LED's face the camera module. The targets position places it within zone #1 of the measurement volume. Axial ($\Delta x_{LCG}$ = -593 mm) and vertical ($\Delta z_{LCG}$ = 213 mm) measurements from the target center to the LCG are made to enable the Krypton software to shift local measurements at the targets origin to the LCG of model 5512. This shift is setup in software and occurs synchronously as data is acquired. 6DOF ascii motion data is reported from the camera controller at 40 Hz. Analog data lines from the loadcell, motion tracker, PMM potentiometers, and carriage speed circuit are run to the drive carriage to an onboard 16-channel AD card and PC.

#### 3.7.1.2 Data Acquisition Procedures

First, at-rest reference voltages are measured for all instruments. Then, the PMM is activated and ten seconds elapse to allow enough time for the motion to reach a steady rate. Next, the carriage is started and accelerates through 10 m to a constant speed. Data acquisition commences after traveling another 10 m which allows the unsteady free surface to develop and reach a state where it is not in transition. Data acquisition occurs at 100 Hz / channel for 30, 20, 10 seconds, respectively, for cases where $Fr$ = 0.138, 0.28, 0.41, respectively. For static drift tests, the PMM remains inactive during the carriage run, however, all other procedures above are followed.

### 3.7.2 Phase-Averaged Flowfield

#### 3.7.2.1 Data Acquisition Setup

The phase-averaged flowfield experimental setup is shown in Fig. 3-11. Model 5512 is ballasted to its dynamic sinkage and trim for $Fr = 0.28$ and mounted on the tank centerline in the fixed condition. The PMM scotch yoke is adjusted for a 327.2 mm sway amplitude and a maximum heading angle of 10.2°. PMM potentiometers are incorporated in the sway carriage and yaw linkage to track the model maneuvers. Potentiometer cabling is run to onboard amplifiers. The SPIV system is assembled on an automated two-axis ($y$, $z$) traverse which slides on the 4 m strongback underneath the PMM carriage in the $x$-coordinate. The laser and lightsheet optics are arranged to deliver a vertical lightsheet in the ($y$, $z$) crossplane.

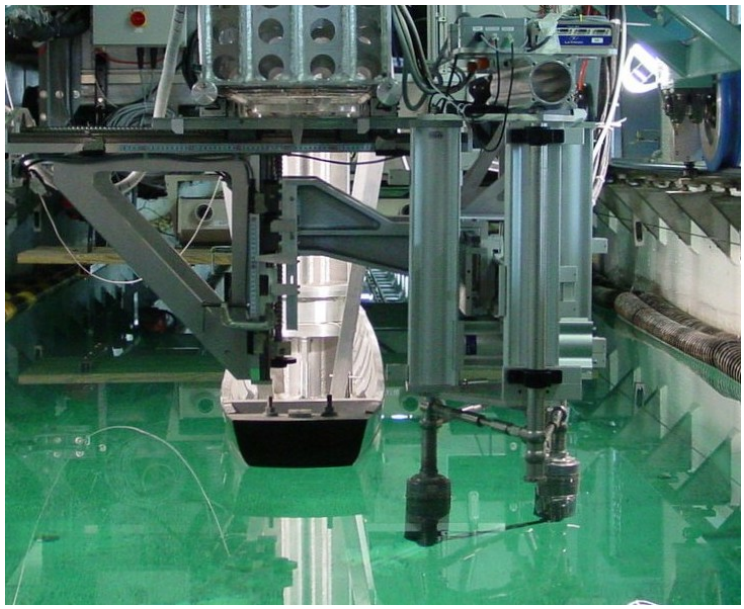

Figure 3-11 Experimental setup for the SPIV flow measurement tests.

Standoff distance between the lightsheet generator and the measurement area center is 553.91 mm (Fig 3-12). The cameras are arranged with equal standoff distances between the enclosures and the measurement area (643.96 mm), 33° of separation between cameras, and a 22° angle between camera #1 and the tank axis to provide clearance with the model and avoid an extremely shallow angle between camera #2 and the cross plane. A minimum separation angle of 30° between cameras is maintained to ensure good measurement quality.

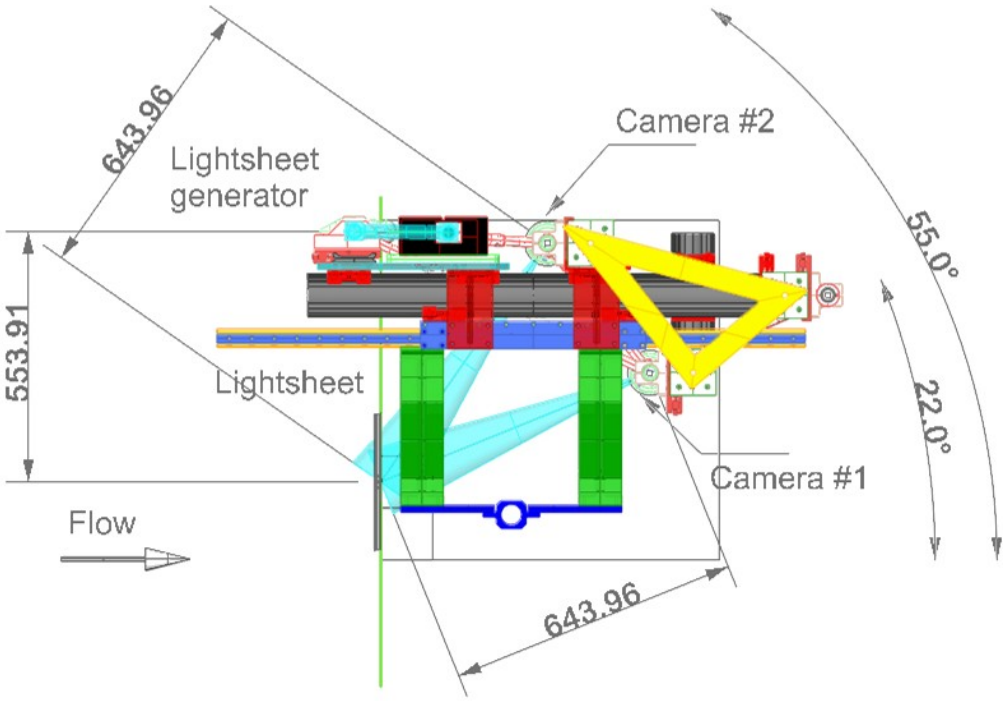


Figure 3-12 Overhead view of the Stereo PIV System.

Power, video, and trigger cables are routed through the strongback to the PIV computer onboard the drive carriage. The laser power supplies ride aboard the PMM carriage. A single umbilical for coolant and electronics cables links the power supplies and the laser head. Laser trigger lines also run through the strongback to the drive carriage

PIV computer. The SPIV computer is equipped with frame grabbers, a programmable timing unit, a TTL/IO board, and an 8-channel AD board capable of synchronously acquiring analog voltages and PIV recordings. An IIHR-designed and -built PIV synchronizer is used to provide equally-spaced trigger pulses to the SPIV computer in order to acquire PIV recordings at presettable, repeatable phase angles in the pure yaw maneuver. This is achieved as the synchronizer monitors the analog output from the PMM sway potentiometer. When a predetermined voltage corresponding to 45° on the rising side of the sway curve is reached, the synchronizer emits a burst of 32 TTL's, each having a 200 μsec pulse width and a time between triggers of 233 ms. Since the pure yaw motion frequency is $f = 0.134$ Hz, this enables a SPIV recording every 11.25° equally spaced through one PMM period. The process is then repeated on subsequent PMM cycles.

#### 3.7.2.2 Data Acquisition Procedures

First, the PMM is activated and ten seconds elapse to allow enough time for the motion to reach a steady rate. A digital oscilloscope monitors the sway carriage analog voltage output and the synchronizer triggers. When they are synched-up, the carriage is started and accelerates through 10 m to a constant speed. Data acquisition commences after traveling another 10 m which allows the unsteady free surface and flowfield to develop and reach a state where they are not in transition. Data acquisition occurs at 4.288 Hz for 19 sec enabling 80-90 SPIV recordings or about 2.5 recordings per each of the 32 phases in the PMM cycle.

At least 100 carriage runs are performed for a given measurement area position to obtain enough recordings at each phase to achieve convergence of the data. Convergence is monitored as the data is acquired and data acquisition is typically stopped when the residual in the velocities drops by two orders of magnitude (Section 4.2). Data acquisition is completed at several overlapping zones at each $x$-station in order to piece together

a complete picture of the region of interest. Four or five zones are used at each *x*-station to cover the region of interest.

## 3.8 Data Reduction Procedures

### 3.8.1 Forces and Moment

Data is processed in batches with a FORTRAN program on a Windows PC. Groups of zero-point and carriage run raw data files are read. Analog voltages are scaled to engineering units with the calibration coefficients and the zero-point correction is computed. For the static drift tests, average values of force and moment are computed from the time histories. For the dynamic tests, the prime frequency of the motion is computed with a fast-Fourier transform (FFT), followed by computation of a $6^{th}$-order FS expansion of the forces and moment. Additionally, the mount-mass effect is computed and subtracted from the dynamic data. For the free-model condition cases, the 6DOF motion of the ship model is analyzed as per the forces and moment harmonic analysis. It is important to note that that $v_{PMM}$, $\dot{v}_{PMM}$, $r_{PMM}$, $\dot{r}_{PMM}$ are not computed with equations (3.1), respectively, but are derived by differentiating potentiometer-measured values of $y_{PMM}$ and $\psi$. All periodic data is expressed and output through one PMM cycle. Finally, the hydrodynamic derivatives are computed as per presented in Section 2 as the last data reduction step.

### 3.8.2 Phase-Averaged Flowfield

SPIV recordings are processed with LaVision DaVis v7.1 software in batch processes. First, the raw images are rotated and mirrored. Then the correlations are completed with one pass using 64 x 64 pixel interrogation windows followed by two passes using 32 x 32 pixel interrogation windows. Fifty percent overlap is used in the horizontal and vertical directions on all correlation passes. A high-accuracy Whitaker reconstruction of the vectors is used in the final pass. Vectors are range filtered using

median values of 0.65, -0.065, 0.065 for ($U$, $V$, $W$), respectively, and bands of ±0.65. A median filter follows, removing vectors if their magnitude is greater than two times the rms value of their neighboring vectors. Spurious vectors are not replaced with interpolated values, and blank spots in the measurement area are not filled. The vector fields and analog voltages (Sanshin sway and yaw and Krypton sway and yaw) are exported and organized according to zone number and carriage run. Then, a FORTRAN program is used to complete the phase-averaging part of the data reduction. Vectors from each carriage run are non-dimensionalized with the measured carriage speeds. Then, the vector fields are sorted into their respective phase groups by analyzing the sway and yaw analog voltage levels associated with each SPIV recording. When the phase-sorting is complete, the phase averaged velocities and Reynolds stresses are computed. The solution for the complete region of interest is stitched together from the multiple zones at the $x$-station. An averaging technique will be used in the overlapping regions of the multiple zones.